Crystal Structure and Resonance Raman Studies of Protocatechuate 3,4-Dioxygenase Complexed with 3,4-Dihydroxyphenylacetate[†,‡]

Timothy E. Elgren,[§,∥] Allen M. Orville,[§,⊥,▽,#] Kimberly A. Kelly,[∥] John D. Lipscomb,[⊥,▽] Douglas H. Ohlendorf,[*,⊥,▽] and Lawrence Que, Jr.[*,▽,○]

Department of Chemistry, Hamilton College, Clinton New York 13323, Departments of Biochemistry (Medical School) and Chemistry and the Center for Metals in Biocatalysis, University of Minnesota, Minneapolis, Minnesota 55455

Received March 25, 1997; Revised Manuscript Received July 7, 1997[⊗]

ABSTRACT: The crystal structure of the anaerobic complex of *Pseudomonas putida* protocatechuate 3,4-dioxygenase (3,4-PCD) bound with the alternative substrate, 3,4-dihydroxyphenylacetate (HPCA), is reported at 2.4 Å resolution and refined to an *R* factor of 0.17. Formation of the active site Fe(III)·HPCA chelated complex causes the endogenous axial tyrosinate, Tyr447 (147β), to dissociate from the iron and rotate into an alternative orientation analogous to that previously observed in the anaerobic 3,4-PCD·3,4-dihydroxybenzoate complex (3,4-PCD·PCA) [Orville, A. M., Lipscomb, J. D., & Ohlendorf, D. H. (1997) *Biochemistry 36*, 10052−10066]. Two orientations of the aromatic ring of HPCA related by an approximate 180° rotation within the active site are consistent with the electron density. Resonance Raman (rR) spectroscopic data from *Brevibacterium fuscum* 3,4-PCD·HPCA complex in solution reveals low frequency rR vibrational bands between 500 and 650 cm^{-1} as well as a band at ∼1320 cm^{-1} which are diagnostic of a HPCA·Fe(III) chelate complex. ^{18}O labeling of HPCA at either the C4 or C3 hydroxyl group unambiguously establishes the vibrational coupling modes associated with the five-membered chelate ring system. Analysis of these data suggests that the Fe(III)−$HPCA^{O4}$ bond is shorter than the Fe(III)−$HPCA^{O3}$ bond. This consequently favors the model for the crystal structure in which the C3 phenolic function occupies the Fe^{3+} ligand site opposite the endogenous ligand $Tyr408^{O\eta}$ (108β). This is essentially the same binding orientation as proposed for PCA in the crystal structure of the anaerobic 3,4-PCD·PCA complex based solely on direct modeling of the $2|F_o| - |F_c|$ electron density and suggests that this is the conformation required for catalysis.

Protocatechuate 3,4-dioxygenase (3,4-PCD)[1] utilizes a mononuclear, non-heme Fe^{3+} center to catalyze reactions of the type shown in Scheme 1. The enzyme has been isolated from many soil bacteria but has been particularly well characterized from *Pseudomonas putida*,[2] *Pseudomonas cepacia*, and *Brevibacterium fuscum* [for reviews see Lipscomb and Orville (1992), Que (1989), and Que and Ho (1996)]. The crystal structure of the enzyme as isolated from *P. putida* has been determined (Ohlendorf et al., 1988, 1994) and shows that the trigonal bipyramidal iron coordination sphere is comprised of $Tyr408^{O\eta}$ and $His460^{N\epsilon 2}$ as equatorial ligands with $Tyr447^{O\eta}$ and $His462^{N\epsilon 2}$ as axial ligands.[3] A solvent molecule (Wat827, a hydroxide ion) completes the equatorial coordination plane. Several previous spectroscopic results indicate that the iron coordination environments in 3,4-PCDs from the other bacterial sources are very similar

[†] This work was supported by grants from the National Institutes of Health to J.D.L. (GM-24689), D.H.O. (GM-46436), and L.Q. (GM-33162). T.E.E. acknowledges the Donors of The Petroleum Research Fund for partial support of this work. A.M.O. acknowledges a NIH predoctoral training grant (GM-07323) and a Doctoral Dissertation Fellowship from the Graduate School, University of Minnesota.

[‡] The coordinates for the 3,4-PCD·HPCA complex have been submitted to the Protein Data Bank (Bernstein et al., 1977) with the submission code 3PCN.

* Authors to whom correspondence should be addressed. Douglas H. Ohlendorf: Department of Biochemistry 4−225 Millard Hall, University of Minnesota, Minneapolis, MN 55455-0347. tel: (612) 624-8436. FAX: (612) 624-5121. E-mail: ohlen@dccc.med.umn.edu. Lawrence Que, Jr.: Department of Chemistry, 139 Smith Hall, University of Minnesota, Minneapolis, MN 55455. tel: (612) 625-0389. Fax: (612) 624-7029. E-mail: que@chemsun.chem.umn.edu.

[§] Joint first authorship.

[∥] Hamilton College.

[⊥] Department of Biochemistry, University of Minnesota.

[▽] Center for Metals in Biocatalysis, University of Minnesota.

[#] Current address: Institute of Molecular Biology, University of Oregon, Eugene, OR 97403.

[○] Department of Chemistry, University Minnesota.

[⊗] Abstract published in *Advance ACS Abstracts,* September 1, 1997.

[1] Abbreviations used: 3,4-PCD, protocatechuate 3,4-dioxygenase; 1,2-CTD, catechol 1,2-dioxygenase; R2-F208Y_{dopa}, ribonucleotide reductase F208Y mutant R2 protein after autocatalytic conversion into dopa208 (Ormö et al., 1992; Åberg et al., 1993); PAH, phenylalanine hydroxylase; hTH, human tyrosine hydroxylase; PCA, 3,4-dihydroxybenzoate or protocatechuate; HPCA, homoprotocatechuate or 3,4-dihydroxyphenylacetate; DHPP, 3,4-dihydroxyphenylpropionate; $HPCA_{(StrA)}$, the atomic model for the 3,4-PCD·HPCA complex in which HPCA C3-phenolate coordinates the iron *trans* to $Tyr408^{O\eta}$; $HPCA_{(Str.\ B)}$, the atomic model for the 3,4-PCD·HPCA complex in which HPCA C4-phenolate coordinates the iron *trans* to $Tyr408^{O\eta}$; PHP, *p*-hydroxyphenylacetate; MHP, *m*-hydroxyphenylacetate; $catH_2$, catechol; NTB, tris(benzimidazolyl-2-methyl)amine; PDA, *N*-(2-pyridylmethyl)iminodiacetate; NTA, *N,N*-bis(carboxymethyl)glycinetriamine; salen, ethylenebis(salicylideneamine) dianion; DOPA, 3,4- dihydroxyphenylalanine; rR, resonance Raman; XANES, X-ray absorption near-edge structure; EXAFS, extended X-ray absorption fine structure; LMCT, ligand to metal charge transfer; rms, root mean squared; F_P and $F_{P\cdot HPCA}$, the observed structure factors for the native and complex of 3,4-PCD, respectively.

[2] American Type Culture Collection (ATCC) 23975, previously classified as *Pseudomonas aeruginosa*.

[3] The amino acid numbering scheme is that utilized in the refinement of the crystal structure of 3,4-PCD as isolated from *P. putida* (Ohlendorf et al., 1994); α-subunits (residues 1−200), β-subunits (residues 301−538), substrate is numbered 550, iron is residue 600, and solvent numbering starts at 601.

S0006-2960(97)00691-0 CCC: $14.00

Scheme 1: General Reaction Catalyzed by 3,4-PCD (Top) with Kinetic Constants (Bottom)[a]

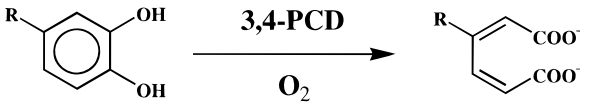

Substrate	R	K_m (μM) organic	K_m (μM) O_2	K_d (μM)	TON s^{-1} $site^{-1}$
PCA	$-COO^-$	30	43	2.5	~ 33
HPCA	$-CH_2COO^-$	6.7	1.2	220	~ 0.15
DHPP	$-CH_2CH_2COO^-$	2.3	4.5	~ 70	~ 0.022

[a] The turnover number (TON) reported for the reactions was measured at 4 °C (PCA) or 24 °C (HPCA and DHPP). [Data compiled from Fujisawa and Hayaishi (1968), Fujisawa et al. (1972, 1973), Que et al. (1977) and Bull et al. (1981).]

to that of *P. putida*, despite quaternary structures that range from $(\alpha\beta Fe^{3+})_4$ to $(\alpha\beta Fe^{3+})_{12}$ (Lipscomb & Orville, 1992) and primary sequence homology within the structural core of the enzymes that ranges from 46−65% identity (Ohlendorf et al., 1994). However, the analogous residues that coordinate the iron (and interact with substrates) in the *P. putida* structures are 100% conserved in the 3,4-PCD family (Ohlendorf et al., 1994; Orville et al., 1997b).

Several crystal structures of 3,4-PCD complexed with competitive inhibitors, protocatechuate (PCA), and substrate analogs were communicated in two previous reports (Orville et al., 1997a,b). Those studies demonstrated that the axial tyrosinate (Tyr447) is dissociated from the Fe^{3+} upon substrate binding as part of a conformational change that yields the chelated Fe^{3+}·PCA complex. In this complex, the reoriented Tyr447 forms the top of a small, bulk solvent excluded cavity, which is proposed to be the O_2 binding site. One side of this cavity includes an open Fe^{3+} ligation site which could be utilized to bind the distal end of a peroxy intermediate during catalysis, thereby promoting O−O bond cleavage, and retaining the distal oxygen for incorporation into the product as required by the dioxygenase stoichiometry (Orville et al., 1997b).

Careful modeling of the substrate to the 2.1 Å resolution electron density in the active site suggested that the Fe^{3+}−PCA^{O3} bond is longer than the Fe^{3+}−PCA^{O4} bond. We postulate that this asymmetry in the Fe^{3+}−$PCA^{catecholate}$ bond lengths derives primarily from *trans* influences of the endogenous iron ligands. This structure would have the mechanistic consequence that the PCA^{O3} would have a greater tendency to ketonize and therefore initial electrophilic attack by O_2 would be directed to the PCA−C4 where negative charge would develop. While the initial attack at PCA−C4 is chemically reasonable and agrees with the current mechanistic hypothesis (Lipscomb & Orville, 1992; Orville et al., 1997b), the critical assignment of the identity of the short Fe^{3+}−$PCA^{catecholate}$ bond is based primarily on our ability to distinguish between subtly different models for the crystal structure of the enzyme·PCA complex.

Another approach to this problem is to make use of resonance Raman (rR) spectroscopy which has been valuable in studies of the iron ligation of 3,4-PCD [reviewed in Que (1989, 1983)] and numerous other iron-containing enzymes with ligands that give rise to ligand to metal charge transfer (LMCT) bands. For example, in the 3,4-PCD isolated from *B. fuscum*, the LMCT bands near 450 nm from the two endogenous tyrosinate ligands give rise to rR features at 1254 and 1266 cm^{-1}, respectively. It has been noted that the formation of a chelated Fe^{3+}·catecholate complex can give rise to distinctive, low-frequency rR features between ~500 and ~640 cm^{-1} that are coupled to the LMCT bands between 600 and 850 nm of these complexes (Öhrström & Michaud-Soret, 1996; Michaud-Soret et al., 1995; Ling et al., 1994; Salama et al., 1978). This has been particularly useful in demonstrating the direct chelation of exogenous catecholic ligands to the ferric ion in phenylalanine hydroxylase (Cox et al., 1988; Michaud-Soret et al., 1995), tyrosine hydroxylase (Michaud-Soret et al., 1995), lipoxygenase (Nelson et al., 1995), and the endogenous dopa residue in the $F208Y_{dopa}$ mutant R2 protein of ribonucleotide reductase (Ormö et al., 1992; Åberg et al., 1993; Ling et al., 1994). The substrate complex of 3,4-PCD also exhibits the 600−850-nm LMCT bands, and consequently this same approach should be useful in the detection of an Fe^{3+}−substrate chelate in the 3,4-PCD·substrate complexes. Moreover, through the use of appropriately mass-labeled substrate analogs, these results may be extended to determine the occurrence and nature of asymmetry in this complex.

Two difficulties in the application of rR spectroscopy to this problem are the relatively broad rR bands observed for *P. putida* 3,4-PCD and the inherent fluorescence that is observed from the PCA complex. These can be respectively addressed through the use of the 3,4-PCD from *B. fuscum*, which gives sharper rR features (Whittaker et al., 1984; Siu et al., 1992), and the use of alternate substrates such as homoprotocatechuate (HPCA) or 3,4-dihydroxyphenylpropionate (DHPP) which elicit less fluorescence. These alternate substrates may also be expected to give sharper rR spectra than the PCA complex because other spectroscopic techniques have shown that their enzyme complexes are much more homogeneous than the 3,4-PCD·PCA complex (Orville & Lipscomb, 1989).

The alternative substrates are turned over slowly to give intradiol cleavage products like PCA (Scheme 1). As shown in Scheme 2, transient kinetic results suggest that the lower turnover numbers for HPCA and DHPP reflect the reduced rates for substrate association and product release (the rate-limiting step) rather than the ring opening reaction itself. Consequently, the structures of final substrate complex and of the intermediates in which the chemical steps occur are likely to be similar in the 3,4-PCD complexes with PCA and the slower substrates. This presumption is supported by the observation of similar optical and magnetic spectroscopic features from all of the anaerobic 3,4-PCD·substrate complexes as well as their reaction cycle intermediates formed after the introduction of O_2. However, the sharper spectra from the enzyme·substrate analog complexes have allowed experiments such as the detection of magnetic hyperfine interactions from labeled analogs by EPR spectroscopy. For example, it was shown that both 3-[^{17}O]HPCA and 4-[^{17}O]HPCA broaden the EPR spectrum, which strongly suggests that a chelated Fe^{3+}·HPCA complex is formed (Orville & Lipscomb, 1989).

In this report, we present the crystal structure of the anaerobic 3,4-PCD·HPCA complex from *P. putida* and correlate it to highly resolved rR spectroscopic data of the same complex formed in solution with the 3,4-PCD isolated

Scheme 2: Kinetic Mechanism Determined for Three Aromatic Substrates at (a) 4 °C (Bull et al., 1981) and at (b) 24 °C (Fujisawa et al., 1972)

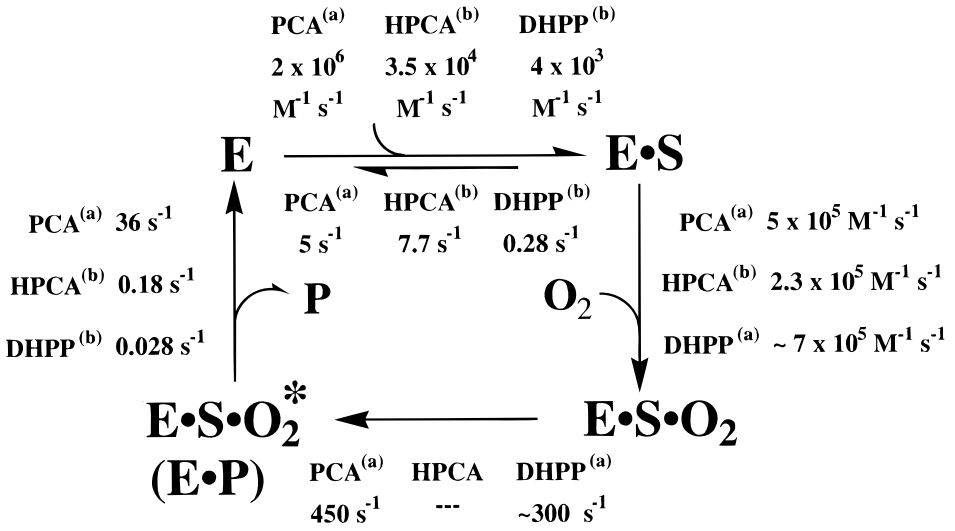

from *B. fuscum*. The crystal structure reveals an asymmetrically chelated Fe^{3+}·HPCA complex. Accordingly, the resonance Raman spectra exhibit the low frequency bands diagnostic of a chelated Fe^{3+}·catecholate complex. Unambiguous assignment of the long and short $Fe^{3+}-O$ bonds in the chelate complex are then made based on rR spectra from ^{18}O-labeled HPCA. The correlation of the spectroscopic and structural data is consistent with our mechanistic proposals and offers further insights into the origin of the relatively slow turnover rate of HPCA.

EXPERIMENTAL PROCEDURES

Isolation of Enzymes. 3,4-PCD was purified from either *P. putida* (ATCC 23975)[2] or *B. fuscum* (ATCC 15993) grown on 4-hydroxybenzoate as the only carbon source according to established procedures (Que et al., 1976; Whittaker et al., 1990). 4-Hydroxyphenylacetate 3-hydroxylase was isolated from *B. fuscum* cultured on PHP as the sole source of carbon and energy (Orville & Lipscomb, 1989; Orville et al., 1990). Enzyme assays were performed with a polarographic oxygen electrode following O_2 consumption (Whittaker et al., 1990).

Crystallization and Structure Determination. Crystals of *P. putida* 3,4-PCD were grown aerobically by vapor diffusion at 4 °C according to Ohlendorf et al. (1994). Two anaerobic 3,4-PCD·HPCA complexes were formed by the method of Orville et al. (1997b). The X-ray diffraction data were collected at 23 °C using the methods described in previous reports (Orville et al., 1997b; Ohlendorf et al., 1994). Data sets from the two anaerobic 3,4-PCD·HPCA complexes were merged and the statistics for data processing and model refinement are reported in Table 1. X-ray reflections to a resolution limit where the average $I/\sigma_I \geq 1$ were retained for model refinement. The idealized atomic model, bond distances, and bond angles for HPCA were obtained from an energy-minimized (DISCOVER) model built with InsightII (Biosym Corporation, La Jolla, CA). Diffraction data with structure factors $\geq 1\sigma$ between 6 and 2.4 Å were used to refine the atomic models (Ohlendorf et al., 1994; Orville et al, 1997b) with PROLSQ (Hendrickson & Konnert, 1980; Hendrickson, 1985) on a Cray Y-MP supercomputer. The starting model for the anaerobic 3,4-PCD·HPCA complex was derived from the refined 3,4-PCD structure (Ohlendorf et al., 1994) from which all the active site solvent molecules had been removed and the axial tyrosine (Tyr447) was rotated into the alternative position indicated by the difference Fourier maps. The atoms in HPCA were restrained to two planes during refinement; bond distances between the Fe^{3+} and coordinating atoms were not restrained during refinement. The final metal−ligand distances are consistent with other protein−transition metal bond distances (Glusker, 1991; Holm et al., 1996) and the iron−ligand distances determined from EXAFS results of the *B. fuscum* 3,4-PCD·HPCA complex (True et al., 1990). The stereochemical quality of the final structures was assessed with the program

Table 1: Data Collection[a] and Model Refinement Summary

Data Collection	
ligand (concentration)	HPCA (75 mM)
resolution cutoff (Å)	2.4
*I*2 unit cell: *a*, *b*, *c* (Å), β angle	196.6, 127.5, 134.3, 97.7°
total observations (unique)	792 401 (127 824)
R_{merge}	0.072[b] (0.110)[c]
$R_{isomorphous}$ to native[d]	0.173
fraction of data (res. shell)	0.97 (10−2.4 Å)
	0.89 (2.5−2.4 Å)
average intensity [$I/\sigma(I)$]	10.0 (10−2.4 Å)

Model Refinement	*Str. A*	*Str. B*
resolution range (Å)	6.0−2.4	6.0−2.4
reflections with $F \geq 1.0\sigma$	100 077	100 077
R factor[e]	(6.0−2.4 Å) 0.166	(6.0−2.4 Å) 0.164
	(2.6−2.4 Å) 0.209	(2.6−2.4 Å) 0.205
rms deviation from ideal		
23 symmetry (Å)	0.154	0.159
bond distances (Å)	0.017	0.017
bond angles	2.8°	2.8°
no. of non-H protein atoms	20,568	20,568
no. of solvent molecules	1,380	1,374
mean *B* values (Å^2)		
α-subunit (β-subunit)	25.4 (19.2)	25.4 (19.2)
HPCA (solvent)	16.6 (20.5)	16.4 (20.6)

[a] Data combined from two crystals. [b] Weighted $R_{merge} = [\Sigma_{hkl}\Sigma_i\{(I_i - \langle I\rangle_i G_i)/\sigma_i\}^2/\Sigma_{hkl}\Sigma_i(I_i/\sigma_i)^2]^{1/2}$. [c] Absolute $R_{merge} = \Sigma_{hkl}\Sigma_i|I_i - \langle I\rangle_i G_i|/\Sigma_{hkl}\Sigma_i I_i$. where, for observation *i* of reflection *hkl*, I_i is the observed intensity, $\langle I\rangle_i$ is its mean intensity, G_i is the scaling function applied, and σ_i is the standard deviation. [d] $R_{isomorphous} = \Sigma_{hkl}|F_{complex} - F_{native}|/\Sigma_{hkl}F_{native}$ where $F_{complex}$ and F_{native} are the structure factors for the 3,4-PCD·HPCA complex and 3,4-PCD as isolated, respectively. [e] *R* factor $= \Sigma_{hkl}|F_o - F_c|/\Sigma_{hkl}F_c$.

WHAT CHECK (Hooft et al., 1996). The atomic coordinates for the R2-F208Y_{dopa} structure (1RNR; Åberg et al., 1993) were obtained from the Protein Data Bank (Bernstein et al., 1977).

Preparation of Labeled Compounds. 3-[^{18}O]HPCA and 4-[^{18}O]HPCA were prepared according to the method of Orville et al. (1990). Labeling at the C4 hydroxyl position was achieved by conversion of 4-aminophenylacetate (Aldrich) to the diazonium salt followed by hydrolysis in ^{18}O-enriched water (99% enriched, Isotec, Inc.). *o*-Hydroxylation of *p*-hydroxyphenylacetate (PHP, Sigma) was catalyzed by PHP 3-hydroxylase, a flavoprotein monooxygenase isolated from *B. fuscum* cultured on PHP using the method of Orville et al. (1990). When the ^{18}O was to be incorporated into the C3 OH position, this enzymatic synthesis was carried out under an $^{18}O_2$ (95%, Cambridge Isotope Laboratories) atmosphere. Purification of PHP and HPCA was achieved with reversed-phase HPLC using an Ultremex 5 C18 column (250 × 10 mm, Phenomenex) with an isocratic mobile phase (89% water, 10% 2-propanol, 1% acetic acid pH ∼ 2.5). Electrospray ionization mass spectral data were collected on a Sciex API III mass spectrometer and confirmed >94% enrichment of ^{18}O for both isotopomers.

Resonance Raman Conditions. Resonance Raman spectra were collected using a Spex model 1403 spectrometer interfaced with a Spex DM3000 data acquisition system. Laser excitation was provided by a Spectra-Physics 2030 argon ion laser or a 375B dye laser using Rhodamine 6G dye (Exciton, Inc.). The laser power measured at the sample was typically ca. 50 mW. The Raman scattering was collected at 90° with a slit width of 4 cm^{-1}. Protein samples for rR studies were prepared in 50 mM MOPS buffer at pH 7.2. These protein samples had Fe^{3+} concentrations of 0.58 mM, determined by absorption at 435 nm ($\epsilon_{435} \approx 2900$ M^{-1} cm^{-1} per iron), corresponding to protein concentrations of 0.12 mM. The anaerobic enzyme−substrate complex was prepared with an HPCA (Sigma) concentration of 25 mM. Anaerobic 3,4-PCD·HPCA samples were sealed in a quartz spinning cell held at ca. 5 °C by a constant stream of cold nitrogen gas. Raman shifts were referenced against the 983 cm^{-1} A_1 stretch of a Na_2SO_4 standard solution.

RESULTS

Crystal Structure of the P. putida Anaerobic 3,4-PCD·HPCA Complex. Formation of the anaerobic 3,4-PCD·HPCA complex turned the burgundy-red crystals of *P. putida* 3,4-PCD dark blue. The crystals were virtually identical in color to anaerobic HPCA complexes formed in solution with enzyme isolated from either *P. putida* (Fujisawa et al., 1972) or *B. fuscum* (Figure 1). X-ray diffraction data from two crystals were collected and merged to yield a nearly complete and highly redundant data set for the complex (Table 1). The R_{merge} for the combined data set is only slightly higher than either individual data set, suggesting that the two are very similar. The $R_{isomorphous}$ magnitude, which is typical of the exogenous ligand complexes of 3,4-PCD (Orville et al., 1997a,b), suggests that the structure of the complex is altered relative to that of the uncomplexed enzyme. On the other hand, the similarity of the unit cell parameters indicates that the complex is isomorphous to uncomplexed 3,4-PCD. The initial $|F_{P\cdot HPCA}| - |F_P|$ difference Fourier maps (not shown) are similar to those observed

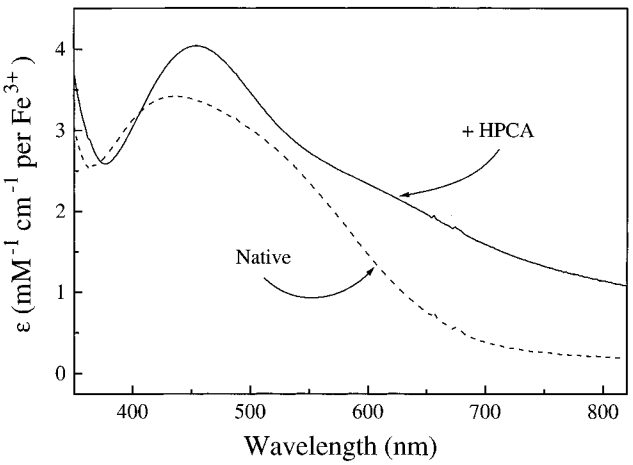

FIGURE 1: Optical absorption spectrum of the *B. fuscum* 3,4-PCD·HPCA complex. 3,4-PCD (∼200 μM Fe^{3+}) was mixed anaerobically with 100 mM HPCA in 50 mM MOPS buffer at pH 7.0. For comparison the spectrum of the enzyme as isolated is also shown (- - -).

in the 3,4-PCD·PCA and substrate analog complexes (Orville et al., 1997b) and reveal conformational changes restricted to the active sites and along the α/β-subunit interfaces. After several rounds of refinement without HPCA or solvent molecules in the active site, HPCA was placed into the active site $|F_o| - |F_c|$ and $2|F_o| - |F_c|$ density in two different orientations. Each model was independently refined further to yield equivalent *R* factors and electron density maps (Figure 2). Therefore, the data are apparently not of sufficient resolution to unambiguously distinguish between homogeneous models of either HPCA orientation.[4] The resolution of the data also does not warrant refining a single atomic model containing both HPCA orientations at 50% occupancy. As shown in Figure 3, the two structures are related to each other by an approximately 180° rotation of the aromatic ring. We present structures of both possible HPCA orientations and refer to them as $HPCA_{(StrA)}$, and $HPCA_{(StrB)}$, for the substrate orientation with $HPCA^{O3}$ or $HPCA^{O4}$ coordinating the Fe^{3+} from the equatorial site *trans* to Tyr408, respectively.

Despite the uncertainty of the HPCA orientation in the active site, formation of the chelated Fe^{3+}·HPCA complex clearly causes the dissociation of Tyr447 from the iron (Figures 2 and 3). Tyr447 is rotated into the alternative orientation previously observed in the 3,4-PCD·PCA and substrate analog complexes (Orville et al., 1997b) and is stabilized by hydrogen bonds with $Tyr16^{OH}$ and $Asp413^{O\delta1}$. $Tyr447^{N}$ and $Tyr447^{O}$ also form hydrogen bonds with $Arg457^{O}$ and $Arg457^{N}$, respectively, while $Asp413^{O\delta2}$ forms a hydrogen bond with $Tyr408^{N}$. An oxygen atom in the acetate group of HPCA in either $HPCA_{(StrA)}$ or $HPCA_{(StrB)}$ forms a hydrogen bond with $Tyr324^{OH}$, albeit at different distances (∼2.5 Å for $HPCA_{(StrA)}$; and ∼ 3.3 Å for $HPCA_{(StrB)}$). Several solvent molecules also hydrogen bond to residues near the HPCA molecule in each structure. Wat605 hydrogen bonds with $His462^{N\delta1}$; Wat606 hydrogen bonds with $Trp400^{N\epsilon1}$, $Tyr16^{N}$, and $Ala13^{O}$; and Wat643 hydrogen bonds with $Tyr408^{O\eta}$.

[4] Similar refinement trials were performed for the 3,4-PCD·PCA and substrate analog complexes (Orville et al., 1997b). For those complexes the orientations reported exhibited distinctly less residual electron density after modeling than for the alternative orientation in which the ring was rotated by 180°.

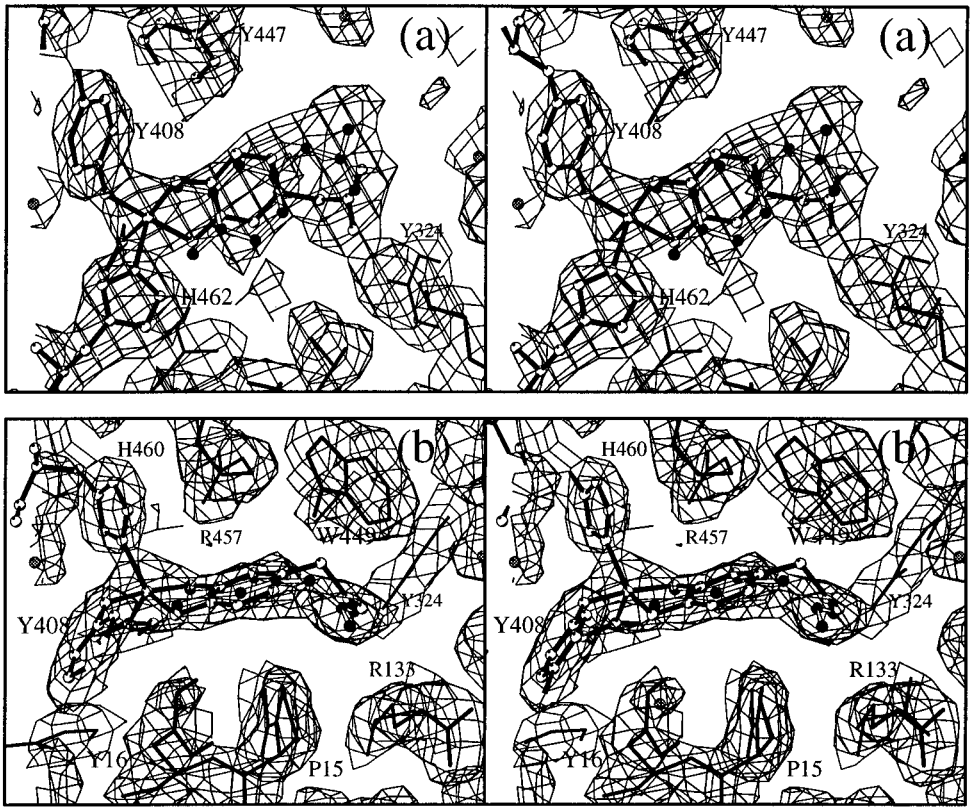

FIGURE 2: Divergent stereoviews of the 6-fold averaged $2|F_o| - |F_c|$ electron density contoured at 1σ for the $HPCA_{(StrA)}$ model (white atoms, black bonds). The $HPCA_{(StrB)}$ model (black atoms, white bonds) yields essentially identical $2|F_o| - |F_c|$ electron density (not shown). The views in a and b are related by a 90° rotation about the horizontal axis. This figure was prepared with MINIMAGE (Arnez, 1994) and MOLSCRIPT (Kraulis, 1991).

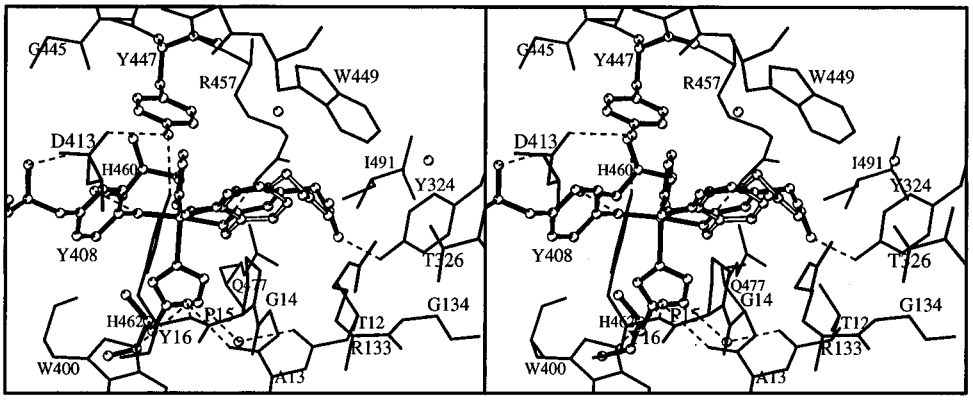

FIGURE 3: Divergent stereoview comparing the two orientations of HPCA in the 3,4-PCD·HPCA complex showing all residues within approximately 6 Å of the HPCA molecules in $HPCA_{StrA}$ (black bonds) and $HPCA_{StrB}$ (white bonds). Hydrogen bonds are indicated by the dashed lines. This figure was prepared with MOLSCRIPT (Kraulis, 1991).

The solvent-exposed surface area for the bound HPCA in $HPCA_{(StrB)}$ (35 $Å^2$, 23% of the total HPCA surface area) is very similar to that in $HPCA_{(StrA)}$ (33 $Å^2$, 21% of the total HPCA surface area). Each is only slightly greater than the 28 $Å^2$ solvent-exposed surface area calculated for PCA bound in the 3,4-PCD active site (Orville et al., 1997b). Several atoms from the acetate group of HPCA in each structure constitute the majority of the solvent exposed surface area. The C3 and C4 atoms of HPCA in both orientations also have solvent-exposed surface areas adjacent to the putative O_2 binding site observed at the PCA^{C3-C4} bond in the 3,4-PCD·PCA complex (Orville et al., 1997b). However, the HPCA binding orientation is rotated relative to PCA, suggesting that the volume of the O_2 cavity is slightly less in the 3,4-PCD·HPCA complexes than in the 3,4-PCD·PCA complex. Moreover, since this is the only solvent-exposed portion of HPCA in each orientation, it appears likely that O_2 attacks from this site, analogous to our proposal for the 3,4-PCD·PCA complex.

The five-coordinate iron geometry in each complex is significantly distorted from either ideal square pyramidal or trigonal bipyramidal coordination geometry (Figure 3 and Table 2). Several obtuse bond angles including that measured between either $His460^{N\epsilon 2}-Fe^{3+}-HPCA^{O4}$ ($HPCA_{(StrA)}$) (146°) or $His460^{N\epsilon 2}-Fe^{3+}-HPCA^{O3}$ ($HPCA_{(StrB)}$) (132°) clearly illustrate the distorted coordination geometry. In the $HPCA_{(StrA)}$ model, the $HPCA^{O3}-Fe^{3+}$ and $HPCA^{O4}-Fe^{3+}$ bond distances are 2.0 and 1.8 Å , respectively. In contrast, the $HPCA_{(StrB)}$ model has 1.7 and 2.1 Å bond distances for the $HPCA^{O3}-Fe^{3+}$ and $HPCA^{O4}$-Fe^{3+} bonds, respectively.

Table 2: Averaged Bond Distances[a] and Angles[b] for the Six Fe^{3+} Centers per Asymmetric Unit

	PCA[c]	$HPCA_{(StrA)}$	$HPCA_{(StrB)}$	MHP[d]	PHP[d]
distance (Å)					
$Tyr408^{O\eta}$−Fe	2.0	1.9	1.9	1.8	1.8
$Tyr447^{O\eta}$−Fe				2.0	1.9
$His460^{N\epsilon2}$−Fe	2.3	2.2	2.2	2.2	2.2
$His462^{N\epsilon2}$−Fe	2.2	2.2	2.2	2.3	2.3
L^{O3}−Fe[e]	2.4	2.0	1.7	1.9	
L^{O4}−Fe[f]	2.2	1.8	2.1		1.8
angle (deg)					
Fe−L^{O3}−L^{C6}	103	103	112	112	
Fe−L^{O4}−L^{C1}	114	106	99		119
$Tyr408^{O\eta}$−Fe−$Tyr447^{O\eta}$				102	103
$Tyr408^{O\eta}$−Fe−$His460^{N\epsilon2}$	90	92	92	97	103
$Tyr408^{O\eta}$−Fe−$His462^{N\epsilon2}$	96	98	101	91	97
$Tyr408^{O\eta}$−Fe−L^{O3}	171	171	94	115	
$Tyr408^{O\eta}$−Fe−L^{O4}	103	88	169		119
$Tyr447^{O\eta}$−Fe−$His460^{N\epsilon2}$				90	90
$Tyr447^{O\eta}$−Fe−$His462^{N\epsilon2}$				166	160
$Tyr447^{O\eta}$−Fe−L^{OH}				84	92
$His460^{N\epsilon2}$−Fe−$His462^{N\epsilon2}$	92	92	95	90	87
$His460^{N\epsilon2}$−Fe−L^{O3}	99	96	132	146	
$His460^{N\epsilon2}$−Fe−L^{O4}	101	146	96		136
$His462^{N\epsilon2}$−Fe−L^{O3}	85	81	131	88	
$His462^{N\epsilon2}$−Fe−L^{O4}	157	122	72		76
L^{O3}−Fe−L^{O4}	75	85	86		

[a] Estimated bond distance errors are ∼0.25 Å based on Luzzati analysis. [b] Estimated bond angle errors are ±3°. [c] From Orville et al. (1997b). [d] From Orville et al. (1997a). [e] The C3−O^- group of HPCA and analogous substituents in the other complexes. [f] The C4−O^- group of HPCA and analogous substituents in the other complexes.

The iron is also approximately 0.4 Å out of the plane of the HPCA aromatic ring in each model. These measurements suggest that regardless of absolute orientation, the HPCA molecule chelates the Fe^{3+} asymmetrically with the longer Fe^{3+}−catecholate bond *trans* to $Tyr408^{O\eta}$. These parameters also suggest that in the trigonal bipyramidal description of the iron coordination sphere, the axial ligand axis is defined by $Tyr408^{O\eta}$ and the exogenous ligand *trans* to it (C3−O in $HPCA_{(StrA)}$ or C4−O in $HPCA_{(StrB)}$). Thus, this axis is rotated ∼90° relative to the iron ligand geometry of uncomplexed 3,4-PCD.

Resonance Raman Spectra of B. fuscum 3,4-PCD·HPCA Complex. The visible absorption spectrum of the anaerobic *B. fuscum* or *P. putida* 3,4-PCD·HPCA complex exhibits low energy catecholate-to-iron charge transfer bands (Figure 1) like those of ferric−catecholate complexes found in other proteins, siderophores, and small molecule metal chelators [*e.g.*, Cox et al. (1988)]. Resonance Raman spectroscopy is an effective technique for exploring the vibrational coupling of the endogenous and exogenous ligands to these LMCT transitions (Que, 1988). Since the rR spectra from the enzyme isolated from *B. fuscum* are the most highly resolved of any 3,4-PCD (Siu et al., 1992), this was the system we focused on for a detailed Raman study. Unfortunately, the inherent fluorescence of the 3,4-PCD·PCA complex has prevented the collection of rR spectra from this species. Although fluorescence is also present in the 3,4- PCD·HPCA complex, it contributes to a much lesser extent than in the PCA complex. The rR spectra of this HPCA complex are also better resolved (Figure 4) than the spectrum reported for the DHPP complex formed with the *P. putida* enzyme (Felton et al., 1978).

The rR spectra in the 900−1700 cm^{-1} region from uncomplexed *B. fuscum* 3,4-PCD, 3,4-PCD·PHP, and 3,4-PCD·HPCA complexes are shown in Figure 4. The rR spectrum in each case exhibits high-frequency bands that are characteristic of Fe^{3+}·phenolate coordination (Siu et al., 1992), whereas only the 3,4-PCD·HPCA complex exhibits bands characteristic of Fe^{3+}·catecholate coordination (the starred peaks in Figure 4c,d) (Michaud-Soret et al., 1995). For example, the uncomplexed enzyme exhibits rR bands at 1254 and 1266 cm^{-1} which derive from the endogenous Tyr408 and Tyr447, respectively (Siu et al., 1992). However, when 578 nm excitation is used (Figure 4a), the high-frequency rR spectrum is dominated by the band associated with Tyr447 because it gives rise to a lower energy LMCT band (Siu et al., 1992). Addition of PHP causes the 1266 cm^{-1} feature to shift to 1288 cm^{-1} and overlaps with the corresponding feature derived from the exogenous ligand (Figure 4b), while the rR band from Tyr408 remains at 1256 cm^{-1} (Siu et al., 1992).

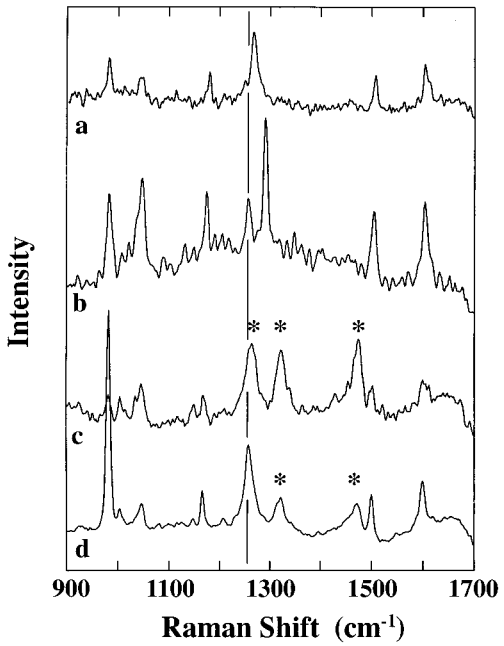

FIGURE 4: The 900−1700 cm^{-1} portion of the rR spectra for (a) *B. fuscum* 3,4-PCD as isolated with 578 nm excitation; (b) the 3,4-PCD·PHP complex with 568 nm excitation; (c) the anaerobic 3,4-PCD·HPCA complex with 580 nm; and (d) 514 nm excitation. The starred features at 1262, 1320, and 1470 cm^{-1} are assigned to catecholate vibrations, while the vertical line denotes the position of the 1256 cm^{-1} bands associated with Tyr408 in the 3,4-PCD·HPCA complex. Other vibrational features of Tyr408 are observed at 1165, 1498, and 1598 cm^{-1}. Other conditions: 4 °C, 50 mM MOPS buffer, pH 7.2; 598 nm laser excitation; 50 mW of laser power, 4 cm^{-1} slit; sum of 30 scans at 5 s/point.

Formation of the anaerobic 3,4-PCD·HPCA complex results in the appearance of a new longer wavelength feature in its visible spectrum (Figure 1), attributed to a catecholate LMCT band. Excitation into this band with 580 nm light affords Raman bands at 1262, 1320, and 1470 cm^{-1} (Figure 4c), features previously shown to be characteristic of a chelated catecholate complex (Salama et al., 1978; Öhrström & Michaud-Soret, 1996). As observed for the tyrosine hydroxylase·dopamine complex (Michaud-Soret et al., 1995) and the DOPA derivative of $R2\text{-}F208Y_{dopa}$ (Ling et al. 1994), these peaks are quite insensitive to the introduction of ^{18}O in the catecholate oxygens, consistent with the notion that these are predominantly catecholate ring modes with only minor contributions from the C−O bonds (Ormö et al., 1992;

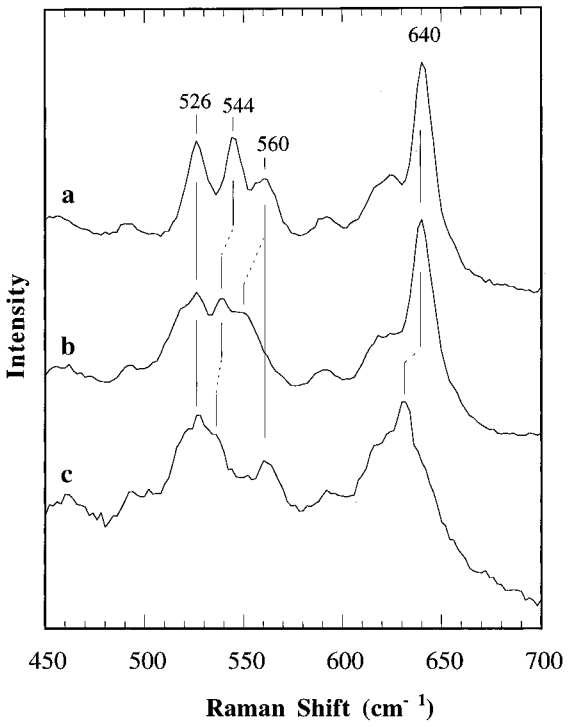

FIGURE 5: Effect of ^{18}O-enriched HPCA on the low-energy Raman features of the anaerobic *B. fuscum* 3,4-PCD·HPCA complex. The complex was formed with unenriched (a) HPCA, (b) 3-[^{18}O]HPCA, or (c) 4-[^{18}O]HPCA. Instrument conditions are given in Figure 4.

Michaud-Soret et al., 1995). When the resonance Raman spectrum of the 3,4-PCD·HPCA complex is obtained with 514 nm excitation (Figure 4d), the catecholate features at 1320 and 1470 cm^{-1} decrease in intensity relative to the spectrum obtained with 580 nm excitation (Figure 4c). This change indicates that the 514 nm laser excitation wavelength has moved out of resonance with the catecholate LMCT band, consistent with earlier studies showing that the catecholate LMCT band is centered in the red region of the visible spectrum (Que & Heistand, 1979). In contrast, the band at ca. 1260 cm^{-1} does not behave in a similar fashion with 514 nm excitation; rather it retains its intensity and shifts to 1256 cm^{-1}. In addition, features at ca. 1165, 1498, and 1598 cm^{-1} become evident. These four features are the fingerprint vibrations of a tyrosinate derived from excitation into a tyrosinate LMCT band at higher energy than the catecholate LMCT band (Que, 1988). Thus the ca. 1260 cm^{-1} peak consists of two overlapping features, one arising from the substrate catecholate and the other from an endogenous tyrosinate. The tyrosinate vibrations arise from Tyr408, consistent with earlier Raman assignments (Siu et al., 1992) as well as the crystal structure of the 3,4-PCD·HPCA complex. No Raman feature is observed from Tyr447 since the rR spectra of a number of inhibitor complexes suggest that Tyr447 should give rise to a unique vibration at ca. 1290 cm^{-1} (Siu et al., 1992). The absence of this feature in the spectra of the 3,4-PCD·HPCA complex is in consonance with its crystal structure showing dissociation of Tyr447 from the iron center upon substrate binding.

Of particular interest in the rR spectrum of the 3,4-PCD·HPCA complex is the low-frequency region from 400 to 700 cm^{-1} (Figure 5 and Table 3) where metal-ligand vibrational modes are routinely found (Nakamoto, 1986). Four prominent bands appear at 526, 544, 560, and 640 cm^{-1} for the 3,4-PCD·HPCA complex. The vibrational band at 526 cm^{-1} is observed in the rR spectrum of uncomplexed 3,4-PCD (Siu et el., 1992) and is therefore not likely to be associated with substrate binding. Isotopic labeling studies demonstrate that the 544 and 560 cm^{-1} bands shift to 538 and 550 cm^{-1}, respectively, when ^{18}O is substituted at the C3 hydroxyl position of HPCA (Figure 5b). Labeling HPCA at the C4 hydroxyl position with ^{18}O results in shifts of the 544 and 640 cm^{-1} bands to 536 and 630 cm^{-1}, respectively (Figure 5c). On the basis of these labeling studies, we can unambiguously assign the two vibrations at 560 and 640 cm^{-1} as arising from ν(Fe−HPCA^{O3}) and ν(Fe−HPCA^{O4}) modes, respectively. The band at 544 cm^{-1} shifts upon ^{18}O substitution at either the HPCA^{O3} or the HPCA^{O4} position, consistent with the assignment of this band as a combination bending and stretching mode of the five-membered ring in the chelated Fe^{3+}·HPCA complex (δ,ν chelate; Öhrström & Michaud-Soret, 1996).

DISCUSSION

We have used X-ray crystallography and resonance Raman spectroscopy to investigate the coordination of the slow substrate, HPCA, to the Fe^{3+} of 3,4-PCD. At 2.4 Å resolution, the electron density is consistent with two orientations of HPCA in the active site. However, no matter which orientation is chosen, the HPCA chelates the iron, causes the dissociation of the endogenous axial tyrosinate ligand (Tyr447), and establishes a new axial ligand axis for the resulting trigonal bipyramidal iron coordination sphere. Consequently, the Fe^{3+}−chelate is asymmetric with the longer Fe^{3+}−catecholate bond *trans* to Tyr408 and along the newly defined axial axis. We show here that the correct structure can be determined by correlating it with the Raman spectroscopic results that unambiguously indicate that the stronger Fe^{3+}−catecholate bond is from HPCA^{O4}. The observation of asymmetric chelation in the anaerobic substrate complex of 3,4-PCD has mechanistic implications and will be discussed in the following sections.

Structural Comparisons to Other 3,4-PCD Ligand Complexes. The crystal structures of 3,4-PCD complexed with PCA (Orville et al., 1997b) or the competitive inhibitors, *m*-hydroxyphenylacetate (MHP) or *p*-hydroxyphenylacetate (PHP) (Orville et al., 1997a), provide structural precedence for both potential HPCA orientations (Figure 6 and Table 2). For example, the positions of the acetate groups from HPCA in HPCA$_{(StrA)}$ and PHP virtually superimpose, as do the positions of the acetate groups of HPCA in HPCA$_{(StrB)}$ and MHP (Figure 6a,b). Because HPCA chelates the Fe^{3+} and monodentate complexes are formed by the inhibitors, the positions of the aromatic rings of these exogenous ligands differ slightly. Nevertheless, the binding orientations of HPCA in HPCA$_{(StrA)}$ and HPCA$_{(StrB)}$ are much more similar to those of MHP and PHP in their 3,4-PCD complexes than to the binding orientation of PCA in the 3,4-PCD·PCA complex (Figure 6c,d). In the crystal structure of the latter complex, PCA coordinates the iron to yield a distorted octahedral coordination sphere in which the PCA^{O3} and PCA^{O4} ligands occupy equatorial and axial sites, respectively. This consequently aligns the aromatic ring of PCA approximately parallel with the iron axial ligand plane. In contrast, in HPCA$_{(StrA)}$ and HPCA$_{(StrB)}$, both orientations of HPCA are rotated relative to that of PCA in the 3,4-PCD·PCA complex so that the HPCA aromatic plane is not parallel to either the iron axial or equatorial ligand plane. For this

Table 3: Selected Resonance Raman Features of Fe^{3+} Chelate Complexes

complex	δ,ν chelate (cm^{-1})	ν(Fe−O) (cm^{-1})		$\Delta\nu$(Fe−O) (cm^{-1})	ref[g]
Fe(NTB)(cat)$^{+}$ [a]	518	630			1
Fe(PDA)(cat)$^{-}$ [b]	523	633			1
Fe(NTA)(cat)$^{2-}$ [b]	526	630			1
Fe(salen)(cat)$^{-}$ [c]	511	614			2
$[Fe(cat)_3]^{3-}$ [b]	533	621			3
PAH·catechol[d]	531	621			1
hTH·catechol[d]	528	619			4
hTH·noradrenalin[d]	530	624	636	12	4
hTH·dopamine[d]	528	592	631	39	4
hTH·3-[^{18}O]dopamine[d]	522	580	629		4
hTH·3,4-[^{18}O]$_2$dopamine[d]	509	578	619		4
R2-F208Y-dopa[e]	512	592	619	27	5
R2-F208Y-3-[^{18}O]dopa[e]	499	584	617		5
3,4-PCD·DHPP[b]	518	581	638	57	6
3,4-PCD·HPCA[f]	544	560	640	80	7
3,4-PCD·3-[^{18}O]HPCA[f]	538	550	640		7
3,4-PCD·4-[^{18}O]HPCA[f]	536	560	630		7

[a] CD_3OD, ambient temperature. [b] H_2O, ambient temperature. [c] CD_3CN, ambient temperature. [d] 4 °C. [e] 90 K. [f] 5 °C. [g] References: (1) Cox et al., 1988; (2) Pyrz et al., 1988; (3) Salama et al., 1978; (4) Michaud-Soret et al., 1995; (5) Ling et al., 1994; (6) Felton et al., 1978; (7) this report.

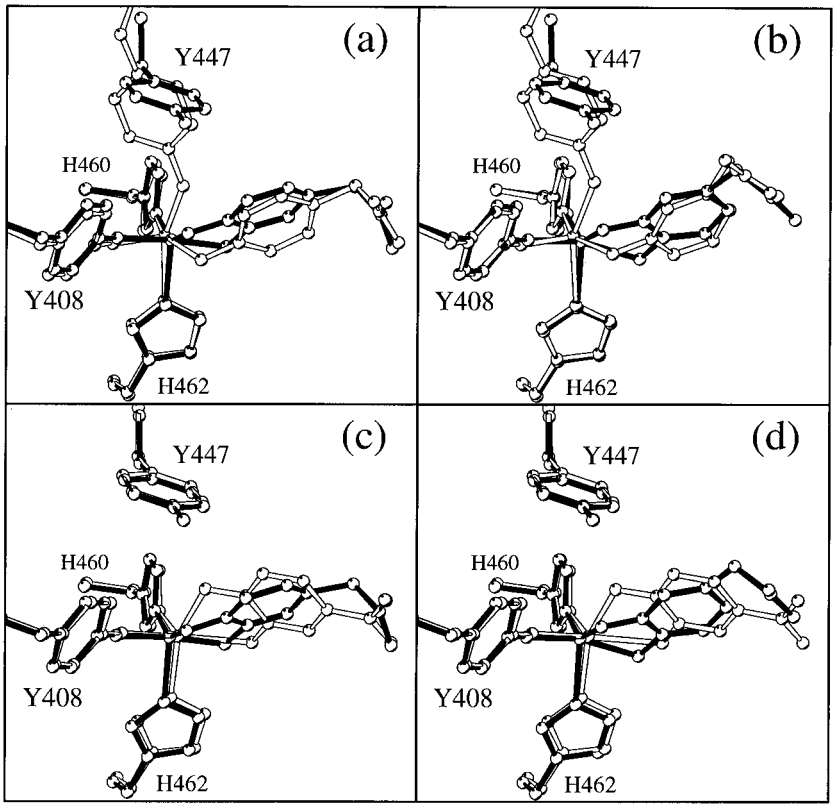

FIGURE 6: Comparison of the Fe^{3+} coordination geometry for 3,4-PCD·HPCA and related complexes. (a) Superposition of 3,4-PCD·PHP (white bonds) and $HPCA_{(StrA)}$ (black bonds); (b) superposition of 3,4-PCD·MHP (white bonds) and $HPCA_{(StrB)}$ (black bonds); (c) superposition of 3,4-PCD·PCA (white) and $HPCA_{(StrA)}$ (black bonds); and (d) superposition of 3,4-PCD·PCA (white bonds) and $HPCA_{(StrB)}$ (black bonds). This figure was prepared with MOLSCRIPT (Kraulis, 1991).

reason, only the phenolic group that coordinates *trans* to Tyr408 in either $HPCA_{(StrA)}$ or $HPCA_{(StrB)}$ superimposes approximately with PCA^{O3} in the 3,4-PCD·PCA complex.

The difference in binding orientations of PCA and HPCA in either model suggests a structural basis for the different kinetic parameters obtained for these substrates (Schemes 1 and 2). Examination of the van der Waals and hydrogen bonding interactions of PCA or HPCA with the active site residues in their respective 3,4-PCD complexes suggests that $HPCA_{(StrA)}$ will have a higher affinity for HPCA than $HPCA_{(StrB)}$. PCA would be predicted to bind tighter than HPCA in either orientation, and this is in accord with the increased K_d for HPCA (~220 μM) relative to PCA (2.5 μM). Transient kinetic analysis shows that the association rate of HPCA is approximately 2 orders of magnitude slower than that of PCA (Bull et al., 1981; Fujisawa et al., 1972). Since both complexes cause a very similar overall conformational change upon binding to 3,4-PCD, the decreased association rate of HPCA may result from a decreased driving force for dissociation of the axial Tyr447 due to the

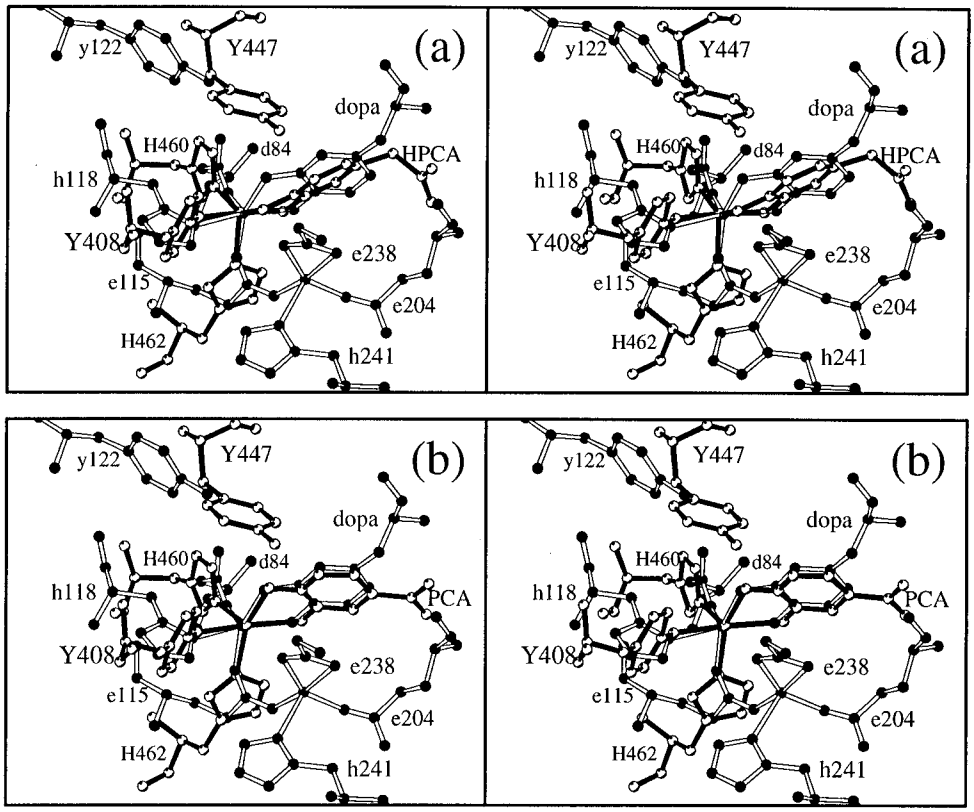

FIGURE 7: Superposition of ribonucleotide reductase R2−F208Y_{dopa} with 3,4-PCD·HPCA or 3,4-PCD·PCA complexes. Divergent stereoviews of (a) $HPCA_{(StrA)}$ (black bonds, white atoms) and R2−F208Y_{dopa} (white bonds, black atoms), (b) 3,4-PCD·PCA (black bonds, white atoms) and R2-F208Y_{dopa}. Uppercase and lowercase labels designate 3,4-PCD or R2-F208Y_{dopa} residues, respectively. This figure was prepared with MOLSCRIPT (Kraulis, 1991).

decreased stability of the final complex. On the other hand, once either E·S complex is formed, the very similar off rates indicate that some step other than the actual release of HPCA from its binding site is rate limiting. One possibility is the rotation of Tyr447 from its alternative binding site and ligation to the Fe^{3+}, which is a process common to both the dissociation of HPCA and PCA.

Structural and Mechanistic Implications of the Resonance Raman Spectra. Formation of a chelated substrate complex is proposed to be essential for the activation of substrate for electrophilic attack by O_2 that leads to intradiol cleavage of catecholic aromatic substrates (Lipscomb & Orville, 1992; Orville et al., 1997b). To date, the best spectroscopic data in support of a chelated Fe^{3+} complex has derived from the evaluation of ^{17}O-enriched HPCA perturbations of the EPR spectrum (Orville & Lipscomb, 1989). However, the low-frequency rR features reported here uniquely arise from the five-membered ring structure formed when the substrate binds in this mode and thus provide a more definitive indication of the chelated binding conformation. Low-energy rR vibrational frequencies for a series of model compounds with this type of Fe^{3+}·catecholate coordination are listed in Table 3 for comparison with the current results as well as those from other proteins that bind catechols.

Chelation of unsubstituted catechols to Fe^{3+} gives rise to two vibrational bands in the low-frequency region: a combination mode associated with the chelated ring between 511 and 526 cm^{-1} and an Fe−O stretching mode between 614 and 633 cm^{-1} (Salama et al., 1978; Michaud-Soret et al., 1995). Density function calculations have been used to describe the combination mode as being comprised of a one-to-one mixture of δ(Fe−O) and ν(Fe−O) vibrations and subsequently termed the δ,ν chelate mode (Öhrström & Michaud-Soret, 1996). Three vibrational bands are observed for *para*-alkyl-substituted, bidentate catecholate complexes (Table 3). Substitution in the *para* position of the catecholate ring removes the degeneracy of the ν(Fe−O) vibrations and both Fe−O stretching modes are observed in addition to the δ,ν chelate mode (Table 3). The isotopic labeling studies of the TH·dopamine complex and R2-F208Y_{dopa} clearly demonstrate that the ν(Fe−$dopa^{O4}$) is at higher energy than the ν(Fe−$dopa^{O3}$).

These assignments are corroborated by the isotope labeling data for the 3,4-PCD·HPCA complex, but the difference in energy between the two ν(Fe−O) bands is significantly larger than for any other complex listed in Table 3. The 640 cm^{-1} band of the 3,4-PCD·HPCA complex [ν(Fe−$HPCA^{O4}$)] is comparatively higher in energy and the 560 cm^{-1} band [ν-(Fe−$HPCA^{O3}$)] lower in energy than those of the other alkyl-substituted catecholate-protein complexes. These differences suggest that the Fe^{3+}·catecholate in the 3,4-PCD·HPCA complex is asymmetrically coordinated with the Fe-$HPCA^{O4}$ bond stronger than the Fe-$HPCA^{O3}$ bond. Moreover, since the crystal structure for the *E. coli* ribonucleotide reductase R2-F208Y_{dopa} (Åberg et al., 1993) is available, the degree of asymmetry in the two catecholate complexes can be directly evaluated. As shown in Figure 7, the superposition of the atomic model for the R2-F208Y_{dopa} (Protein Data Bank entry code 1RNR) with either the $HPCA_{(StrA)}$ or the 3,4-PCD·PCA structure reveals that the F208Y_{dopa} chelate complex is indeed more symmetric than that of either PCA or HPCA bound in 3,4-PCD.

On the basis of this analysis and the fact that the $HPCA_{(StrA)}$ is the orientation most similar to that proposed

for the 3,4-PCD·PCA complex (Figure 6c), it appears that this may be the catalytically relevant species. The long Fe^{3+}-catecholate bond *trans* to Tyr408 appears to derive in part from the effect of placing two anionic ligands *trans* to each other. We proposed in a previous report (Orville et al., 1997b) that the asymmetry in the Fe^{3+}·substrate complex is essential for substrate activation and subsequent events in catalysis. The current results appear to corroborate this proposal. These *trans* ligand effects are proposed to enhance catalysis by weakening the $Fe-O^{catecholate}$ bond *trans* to Tyr408 relative to that *trans* to His462, thereby promoting the ketonization at the substrate C3 carbon required by the proposed mechanism. Since the *trans* ligands to the $F208Y_{dopa}$ residue in R2 are His118 and Asp115 (the bridging carboxylate), the driving force for creating asymmetry in the chelated Fe^{3+}·catecholate is not as strong as in 3,4-PCD. To the extent that this asymmetry is important in the creation of a catecholate susceptible to electrophilic attack by O_2, the R2-$F208Y_{dopa}$ would be less likely to efficiently initiate this aspect of intradiol ring cleavage process.

It is interesting to note that in the superposition shown in Figure 7, the putative oxygen binding cavity of 3,4-PCD-substrate complex aligns with the site between the two irons where oxygen is thought to bind in reduced R2. In the 3,4-PCD turnover cycle we have proposed that this site is used to bind the distal oxygen of a peroxy intermediate occurring after initial O_2 attack on the substrate (Orville et al., 1997b). Subsequently, another *trans* influence involving His460 is postulated to stabilize the transition state during the heterolytic cleavage of the peroxo O−O bond. It is conceivable the putative O_2 binding site of R2 site could be used to promote O−O bond cleavage in a peroxy intermediate of R2-$F208Y_{dopa}$ in the same way. However, the analogous residue in the R2-$F208Y_{dopa}$ structure is Asp84 which is less likely than histidine to stabilize the developing negative charge on the distal oxygen necessary for heterolytic O−O bond cleavage and concomitant Criegee type insertion of the proximal oxygen into the aromatic ring.

ACKNOWLEDGMENT

We thank Steve Oh for assistance in large scale bacterial growths and purification of 3,4-PCD from *B. fuscum*. We are grateful to the Minnesota Supercomputer Center for providing computational resources on the Cray Y-MP.

REFERENCES

Åberg, A., Ormö, M., Nordlund, P., & Sjöberg, B.-M. (1993) *Biochemistry 32*, 9845−9850.

Arnez, J. G. (1994) *J. Appl. Crystallogr. 27*, 649−653.

Bernstein, F. C., Koetzle, T. F., Williams, G. J. B., Meyer, E. F., Jr., Brice, M. D., Rodgers, J. R., Kennard, O., Shimanouchi, T., & Tasumi, M. (1977) *J. Mol. Biol. 112*, 535−542.

Bull, C., Ballou, D. P., & Otsuka, S. (1981) *J. Biol. Chem. 256*, 12681−12686.

Cox, D. D., Benkovic, S. J., Bloom, L. M., Bradley, F. C., Nelson, M. J., Que, L., Jr., & Wallick, D. E. (1988) *J. Am. Chem. Soc. 110*, 2026−2032.

Felton, R. H., Cheung, L. D., Phillips, R. S., & May, S. W. (1978) *Biochem. Biophys. Res. Commun. 85*, 844−850.

Felton, R. H., Barrow, W. L., May, S. W., Sowell, A. L., & Goel, S. (1982) *J. Am. Chem. Soc. 104*, 6132−6134.

Fujisawa, H., & Hayaishi, O. (1968) *J. Biol. Chem. 243*, 2673−2681.

Fujisawa, H., Hiromi, K., Uyeda, M., Nozaki, M., & Hayaishi, O. (1971) *J. Biol. Chem. 246*, 2320−2321.

Fujisawa, H., Hiromi, K., Uyeda, M., Okuno, S., Nozaki, M., & Hayaishi, O. (1972) *J. Biol. Chem. 247*, 4422−4428.

Glusker, J. P. (1991) *Adv. Protein Chem. 42*, 1−76.

Hendrickson, W. A. (1985) *Methods Enzymol. 115*, 252−270.

Hendrickson, W. A., & Konnert, J. H. (1980) in *Biomolecular Structure, Function, Conformation and Evolution* (Srinvasan, R., Ed.) Vol. 1, pp 43−47, Pergamon, Oxford.

Holm, R. H., Kennepohl, P., & Solomon, E. I. (1996) *Chem. Rev. 96*, 2239−2314.

Hooft, R. W. W., Vriend, G., Sander, C., & Abola, E. E. (1996) *Nature 381*, 272.

Kraulis, P. J. (1991) *J. Appl. Cryst. 24*, 946−950.

Ling, J. S., Sahlin, M., Sjöberg, B.-M., Loehr, T. M., & Sanders-Loehr, J. (1994) *J. Biol. Chem. 269*, 5595−5601.

Lipscomb, J. D., & Orville, A. M. (1992) in *Metal Ions in Biological Systems* (Sigel, H., & Sigel, A., Eds.) Vol. 28, pp 243−298, Marcel Dekker Inc., New York.

Michaud-Soret, I., Andersson, K. K., Que, L., Jr., & Haavik, J. (1995) *Biochemistry 34*, 5504- 5510.

Nakamoto, K. (1986) in *Infrared and Raman Spectra of Inorganic and Coordination Compounds*, Wiley-Interscience, New York.

Nelson, M. J., Brennan, B. A., Chase, D. B., Cowling, R. A., Groove, G. N., & Scarrow, R. C. (1995) *Biochemistry 34*, 15219−15229.

Ohlendorf, D. H., Lipscomb, J. D., & Weber, P. C. (1988) *Nature 336*, 403−405.

Ohlendorf, D. H., Orville, A. M., & Lipscomb, J. D. (1994) *J. Mol. Biol. 244*, 586−608.

Öhrström, L., & Michaud-Soret, I. (1996) *J. Am. Chem. Soc. 118*, 3283−3284.

Ormö, M., deMaré, F., Regnström, K., Åberg, A., Sahlin, M., Ling, J., Loehr, T. M., Sanders-Loehr, J., & Sjöberg, B-M. (1992) *J. Biol. Chem. 267*, 8711−8714.

Orville, A. M., Harpel, M. R., & Lipscomb, J. D. (1990) *Methods Enzymol. 188*, 107−115.

Orville, A. M., & Lipscomb, J. D. (1989) *J. Biol. Chem. 264*, 8791−8801.

Orville, A. M., Elango, N., Lipscomb, J. D., & Ohlendorf, D. H. (1997a) *Biochemistry 36*, 10039−10051.

Orville, A. M., Lipscomb, J. D., & Ohlendorf, D. H. (1997b) *Biochemistry 36*, 10052−10066.

Pyrz, J. W., Roe, A. L., Stern, L. J., & Que, L., Jr. (1985) *J. Am. Chem. Soc. 107*, 614−620.

Que, L., Jr. (1983) *Adv. Inorg. Biochem.* 5, 167−199

Que, L., Jr. (1988) in *Biological Applications of Raman Spectroscopy* (Spiro, T. G., Ed.) Vol. 3, pp 491−521, Wiley, New York.

Que, L., Jr. (1989) in *Iron Carriers and Iron Proteins (*Loehr, T. M., Ed.) pp 467−524, VCH, New York.

Que, L., Jr., & Heistand, R. H., III (1979) *J. Am. Chem. Soc. 101*, 2219−2221.

Que, L., Jr., & Ho, R. Y. N. (1996) *Chem. Rev. 96*, 2607−2624.

Que, L., Jr., Lipscomb, J. D., Münck, E., & Wood, J. M. (1977) *Biochim. Biophys. Acta 485*, 60−74.

Que, L., Jr., Lipscomb, J. D., Zimmermann, R., Münck, E., Orme-Johnson, N. R., & Orme- Johnson, W. H. (1976) *Biochim. Biophys. Acta 452*, 320−334.

Salama, S., Stong, J. D., Neilands, J. B., & Spiro, T. G. (1978) *Biochemistry 17*, 3781−3785.

Siu, D. C.-T., Orville, A. M., Lipscomb, J. D., Ohlendorf, D. H., & Que, L., Jr. (1992) *Biochemistry 31*, 10443−10448.

True A. E., Orville, A. M., Pearce, L. L., Lipscomb, J. D., & Que, L., Jr. (1990) *Biochemistry 29*, 10847−10854.

Whittaker, J. W., & Lipscomb, J. D. (1984) *J. Biol. Chem. 259*, 4487−4495.

Whittaker, J. W., Lipscomb, J. D., Kent, T. A., & Münck, E. (1984) *J. Biol. Chem. 259*, 4466- 4475.

Whittaker, J. W., Orville, A. M., & Lipscomb, J. D. (1990) *Methods Enzymol. 188*, 82−88.

BI970691K